



Performance of a plate-wave energy converter integrated in a floating breakwater

Siming Zheng^{1,2}  | Mike Meylan³ | Xiantao Zhang⁴  | Gregorio Iglesias^{2,5} | Deborah Greaves²

¹ State Key Laboratory of Hydrosience and Engineering, Tsinghua University, Beijing, China

² School of Engineering, Computing and Mathematics, University of Plymouth, Drake Circus, Plymouth, UK

³ School of Mathematical and Physical Sciences, The University of Newcastle, Callaghan, Australia

⁴ State Key Laboratory of Ocean Engineering, Shanghai Jiao Tong University, Shanghai, China

⁵ MaREI, Environmental Research Institute & School of Engineering, University College Cork, College Road, Cork, Ireland

Correspondence

Xiantao Zhang, State Key Laboratory of Ocean Engineering, Shanghai Jiao Tong University, Shanghai 200240, China.
Email: zhxt@sjtu.edu.cn

Funding information

2020 Research Program of Sanya Yazhou Bay Science and Technology City, Grant/Award Number: SKJC-2020-01-006; Open Research Fund Program of State key Laboratory of Hydrosience and Engineering (Tsinghua University), Grant/Award Number: sklhse-2021-E-02; European Union funded Marine-I (2nd phase) project, Grant/Award Number: 05R18P02816; Open Research Fund Program of State Key laboratory of Ocean Engineering (Shanghai Jiao Tong University), Grant/Award Number: 1916; Hainan Provincial Natural Science Foundation of China, Grant/Award Number: 520QN290

Abstract

A plate-wave energy converter (pWEC) moored in front of a floating stationary breakwater is considered. The pWEC is composed of a submerged flexible plate with piezoelectric layers bonded to both faces of it. Hence the elastic motion of the plate excited by water waves can be transformed into useful electricity due to the piezoelectric effect. To evaluate the performance of the breakwater-attached pWEC in terms of wave power absorption and wave attenuation, a hydroelastic model based on linear potential flow theory and the eigenfunction matching method is developed with the electromechanical and the hydrodynamic problems of the pWEC coupled together. The pWEC can be either simply supported or clamped at the edge. A multi-parameter analysis is carried out with the employment of the present model. Effects of the width, submergence and edge types of the plate, together with the scales of the breakwater, including its width and draft, on wave power absorption and wave attenuation, are examined. As the pWEC moves towards a deeper position, the main peaks of the frequency response of the wave power absorption efficiency become lower and narrower. In contrast, its effect on wave attenuation is limited.

1 | INTRODUCTION

Since the 1790s, many concepts for wave energy conversion have been proposed [1], the majority of which can be classified into five types: oscillating water column (OWC), overtopping device, point absorber, oscillating wave surge converter and raft-type device. Nevertheless, only a small range of wave energy converters have been tested at large scale and deployed

in the sea [2]. The cost of power and survivability are two significant challenges that need to overcome to increase the commercial competitiveness of wave energy converters (WECs) in the global energy market.

To enhance the economics of the WECs and meanwhile improve their survivability, an effective way is to integrate them into coastal structures, such as breakwaters, jetties and piers or along sections of the coast, which would provide cost-sharing

This is an open access article under the terms of the [Creative Commons Attribution](https://creativecommons.org/licenses/by/4.0/) License, which permits use, distribution and reproduction in any medium, provided the original work is properly cited.

© 2021 The Authors. *IET Renewable Power Generation* published by John Wiley & Sons Ltd on behalf of The Institution of Engineering and Technology

benefits, including construction, installation and maintenance [3, 4].

So far, most of the studies associated with integrating WECs into coastal structures have been focused on the OWC, overtopping and point absorber concepts.

Evans and Porter [5] studied the performance of an onshore OWC device composed of a thin vertical surface-piercing lip in front of a vertical wall. Their theoretical studies demonstrated that the incident wave power could be captured efficiently by choosing proper submergence of the lip and the spacing distance between the lip and the wall. To investigate the performance of OWCs installed along a straight coast/breakwater, Martins-Rivas and Mei [6] and Zheng et al. [7, 8] developed three-dimensional (3D) theoretical models and revealed that wave power extraction from the coast/breakwater integrated OWCs for a certain range of wave conditions can be significantly enhanced due to the constructive coast/breakwater reflection effect. He et al. [9] investigated the performance of a pile-supported OWC breakwater. They found that optimising power take-off damping for maximum power could lead to both satisfactory power extraction and wave transmission. Some other studies related to the integration of OWCs with coastal structures can be found in [10–16].

The hydrodynamic problem for the overtopping device is complicated. Most of the studies related to the integration of that device with coastal structures have been carried out using numerical simulation or/and physical model tests. An Overtopping Breakwater for Energy Conversion (OBREC) was designed to fully utilise traditional breakwaters and capturing wave energy [17]. Vicinanza et al. [17] carried out a series of physical tests of a 2-D OBREC model, discussed the wave loadings and average wave overtopping rate at its rear and front sides, and proposed a new design method for horizontal force on OBREC upper crown wall. Following their work [17], more recently, Contestabile et al. [18] completed the analysis on OBREC geometric parameter variation, with particular interest to the influence of the draft length, the reservoir width and the shape of the front ramp, and extended the overall knowledge on the device behaviour. The loading acting on the flat ramp was found to be greater than the curved ramp in almost all the tests by about 30–40%. Musa et al. [19] analysed the wave flow over the OBREC with the utilisation of FLOW 3D software and obtained a similar trend of the overtopping discharge when compared with the experimental data. Di Lauro et al. [20] performed numerical simulations based on the model IH2VOF, and studied the hydraulic performance and stability response of an OBREC device integrated into a vertical structure. The reflection coefficients of the OBREC were observed to be lower than those computed in front of the traditional breakwater. Comprehensive reviews associated with the OBREC can be found in [3, 21].

The integration of point absorbers into coastal structures has also been the object of recent work. Schay et al. [22] studied the hydrodynamic performance of a heaving point absorber near a fixed vertical wall in regular and irregular

seas with a boundary element method (BEM)-based software. Ning et al. [23] proposed an integrated system of a vertical pile-restrained floating breakwater working under the principle of a point absorber. The experimental test demonstrated that the system's capture width ratio was approximately 24%, whereas the transmission coefficient was lower than 0.50 with a proper power take-off damping force applied. More recently, Ning et al. [24], Zhao et al. [25] and Konispoliatis and Mavrakos [26] studied an array of point absorbers in front of a breakwater by using a BEM-based numerical code, physical testing and a theoretical model, respectively. Instead of focusing on the integration of point absorbers into a conventional plane breakwater, Zhang and Ning [27] considered a novel breakwater with parabolic openings for wave energy harvesting. Their numerical studies showed that the reflected waves from the parabolic opening could travel towards a fixed focus position, stimulating wave power absorption of the point absorbers.

In addition to the five dominant types consisting of rigid bodies, there are some other WECs made from flexible structures, for example elastic plate [28] and bulge wave [29], which may offer improved performance/survivability and reduced cost compared with steel/concrete alternatives.

Zheng et al. [30, 31] proposed analytical models to study wave power absorption/dissipation of an array of floating/submerged porous elastic plates. Assuming the porosity of the elastic plates works as a simplified power take-off system, a profound potential of elastic plates was demonstrated for wave power extraction. The hydroelasticity of a porous elastic plate in other circumstances, for example in two-layer fluids and in front of a vertical wall, was investigated by some other researchers [32, 33]. In fact, an elastic plate with piezoelectric layers bonded to both faces of the flexible substrate can extract energy from ocean waves [28]. Thanks to the piezoelectric effect, the tension variations at the plate-water interface of the plate WEC (pWEC) can be converted into a voltage, and the wave power is ultimately transformed into useful electricity. Renzi [28] developed a coupled hydro-electromechanical model, and evaluated the wave power absorption of a two dimensional (2D) submerged offshore stand-alone piezoelectric plate. Recently, this model was extended by Zheng et al. [34] to study the 3D hydroelastic problem of a circular stand-alone submerged piezoelectric pWEC. Buriani & Renzi [35] considered a submerged pWEC attached in front of a bottom-seated breakwater. It was demonstrated that the performance of the pWEC could be significantly improved due to the presence of the breakwater.

By contrast to the traditional bottom-seated breakwaters, floating breakwaters have less environmental impact since water and sediment are permitted to exchange between their seaside and leeside. Athanassoulis and Mamis [36] investigated a terminator-type piezoelectric system extracting electric energy from the direct impact of water waves impinging upon a vertical cliff, which could be formed by a floating breakwater. The wave power absorption of a cliff integrated piezoelectric system was reported to be as high as 30–50% for appropriate hydro/piezo/electric parameters. Liu and Huang [37]

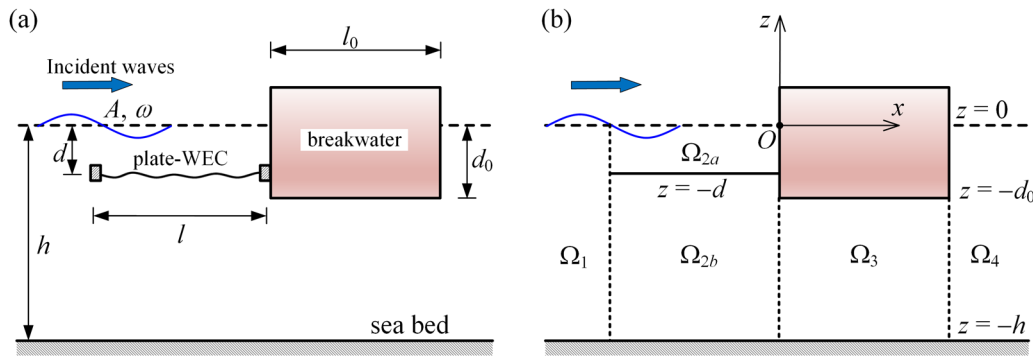


FIGURE 1 Schematic diagram of a floating breakwater integrated pWEC: (a) side view in physical variables; (b) fluid domain decomposition used in the mathematical model.

considered the integration of piezoelectric material with a floating vertical flexible membrane breakwater and developed a theoretical model to study the performance of the system. It was revealed that the proposed system was suitable only at sites where the variability in the wave period is low due to the sensitivity of the transmission coefficient and the output power density on wave periods. This paper considers a floating breakwater integrated piezoelectric pWEC. A 2D theoretical model is developed based on linear potential flow theory and the eigenfunction matching method to study the hydrodynamic performance of the system in terms of wave power absorption and wave attenuation. The proposed model is first validated by comparing the present results with published data and then applied to examine the effect of the width, submergence and edge conditions (i.e. simply supported and clamped) of the pWEC and the width and draft of the breakwater on wave power absorption and wave attenuation.

The rest of this paper is organised as follows: Section 2 outlines the mathematical model for the hydroelastic problem. Convergence analysis and validation of the present theoretical model are given in Sections 3 and 4, respectively. The validated model is then applied to carry out a multi-parameter study on the performance of the floating breakwater integrated pWEC in terms of wave power absorption and wave attenuation, the results of which can be found in Section 5. Finally, conclusions are drawn in Section 6.

2 | MATHEMATICAL MODEL

A pWEC moored in front of a floating stationary breakwater subjected to regular waves of amplitude \mathcal{A} and angular frequency ω is considered (see Figure 1). The waves propagate perpendicularly to the breakwater (i.e. wave crest-line is parallel with the breakwater). The pWEC is made from a flexible substrate with two piezoelectric layers bonded to both faces [28, 34]. The thicknesses of the substrate and the piezoelectric layers are much smaller compared with wavelength and water depth. Hence the pWEC may be assumed of negligible thickness in the

hydrodynamic problem. The floating breakwater is assumed to be strictly constrained that its motion can be neglected, and it is considered stationary in the present work.

As shown in Figure 1, Cartesian axes are chosen with the mean freesurface and front vertical wall of the breakwater coinciding with the planes of $z = 0$ and $x = 0$, respectively, x and z measured in the direction of wave propagation and vertically upwards, respectively. The length of the breakwater and the pWEC in the y -direction is assumed to be far longer than a wavelength so that the hydroelastic problem can be treated as a 2D one. The sea bed is at $z = -h$, and the pWEC with a width l is placed at $z = -d$. The width and draft of the breakwater are denoted by l_0 and d_0 , respectively. The fluid domain is divided into five regions (Figure 1(b)), which we will use in the solution process, that is Ω_1 , the seaside outer region ($x \in (-\infty, -l)$, $z \in [-b, 0]$); Ω_{2a} , the region above the pWEC ($x \in [-l, 0]$, $z \in [-d, 0]$); Ω_{2b} , the region below the pWEC ($x \in [-l, 0]$, $z \in [-b, -d]$); Ω_3 , the region under the floating breakwater ($x \in [0, l_0]$, $z \in [-b, -d_0]$) and Ω_4 , the leeside outer region ($x \in [l_0, \infty)$, $z \in [-b, 0]$).

2.1 | Problem formulation

All amplitudes are assumed to be small enough that linear theory applies, and the fluid is assumed to be inviscid, incompressible and irrotational. It is further assumed that all motion is time-harmonic with the angular frequency ω ; hence the fluid velocity potential and the displacement of the plate about $z = -d$ may be expressed by

$$\Phi(x, z, t) = \text{Re}\{\phi(x, z)e^{-i\omega t}\}, \quad (1)$$

and

$$\tilde{\xi}(x, t) = \text{Re}\{\xi(x)e^{-i\omega t}\}, \quad (2)$$

where Re denotes the real part. The functions $\phi(x, z)$ and $\xi(x)$ represent the time-independent parts of the complex velocity potential and the plate displacement, respectively.

Under the assumptions above, the spatial velocity potential satisfies the Laplace equation in the fluid with the boundary conditions

$$\partial_{\tilde{x}}\phi = \frac{\omega^2}{g}\phi \text{ on } \tilde{x} = 0, x \in (-\infty, 0] \cup [l_0, \infty) \quad (3)$$

$$\partial_{\tilde{x}}\phi = 0 \text{ on } \tilde{x} = -b \quad (4)$$

$$\partial_{\tilde{x}}\phi = 0 \text{ on } \tilde{x} = -d_0, x \in [0, l_0] \quad (5)$$

$$\partial_x\phi = 0 \text{ on } x = 0 \text{ and } l_0, \tilde{x} \in [-d_0, 0] \quad (6)$$

$$\partial_{\tilde{x}}\phi \Big|_{\tilde{x}=-d_+} = \partial_{\tilde{x}}\phi \Big|_{\tilde{x}=-d_-} \text{ on } x \in [-l, 0] \quad (7)$$

where + and - denote above and below the plate, respectively. The scattered wave field consists of outgoing waves only with a finite value at $|x| = \infty$.

Additionally, the time-independent spatial velocity potential, ϕ , at the interface of the regions Ω_{2a} and Ω_{2b} should be coupled to the plate displacement function, ξ , in terms of both kinematic and dynamic conditions [28],

$$\partial_{\tilde{x}}\phi = -i\omega\xi \text{ on } x \in [-l, 0], \tilde{x} = -d, \quad (8)$$

$$g\chi \left(1 + \frac{\beta^2 \zeta \omega}{i + \zeta \omega} \right) \partial_x^4 \xi - \omega^2 \gamma \xi = i\omega(\phi_- - \phi_+) \text{ on } x \in [-l, 0], \tilde{x} = -d, \quad (9)$$

in which + and - denote above and below the plate, respectively;

$$\chi = \frac{B'}{\rho g}, \beta = \frac{\theta'}{\sqrt{B'C'}}, \zeta = \frac{C'}{G'}, \gamma = \frac{I'_b}{\rho}, \quad (10)$$

where B' represents the flexural rigidity of the bimorph, θ' is a piezoelectric coupling factor, C' denotes the electrical surface capacitance, G' is the surface conductance, I'_b represents the surface density of the bimorph, $I'_b = \rho_0 d_0 + 2\rho_p d_p$, in which ρ_0 and ρ_p denote the densities of the substrate and the piezoelectric layers, respectively. d_0 and d_p represent the thicknesses of the substrate and the piezoelectric layers, respectively. ρ is the fluid density. The bimorph piezoelectric plate is characterised by $d_0 = 0.01$ m, $d_p = 1.1 \times 10^{-4}$ m, $\rho_0 = 1250$ kg/m³, $\rho_p = 1780$ kg/m³ (for details see [38] and [28]).

The two components as given above can be combined into

$$\left[\chi \left(1 + \frac{\beta^2 \zeta \omega}{i + \zeta \omega} \right) \partial_x^4 - \frac{\omega^2}{g} \gamma \right] \partial_{\tilde{x}}\phi + \frac{\omega^2}{g} (\phi_+ - \phi_-) = 0 \text{ on } x \in [-l, 0], \tilde{x} = -d, \quad (11)$$

which couples the electro-mechanical and the hydrodynamic problems at the plate-water interface.

We also need to apply edge conditions at the plate end. If the plate is simply supported, the edge conditions are

$$\xi(0) = \partial_x^2 \xi(0) = \xi(-l) = \partial_x^2 \xi(-l) = 0 \quad (12)$$

and they read

$$\xi(0) = \partial_x \xi(0) = \xi(-l) = \partial_x \xi(-l) = 0 \quad (13)$$

for a plate whose edge is clamped.

2.2 | Expressions of the velocity potentials in different regions

2.2.1 | Regions Ω_1 and Ω_4

The eigenfunction expansion in these regions is completely standard and follows from [39, 40], and we only summarise the results here.

Region Ω_1 $\{x \in (-\infty, -l], \tilde{x} \in [-b, 0]\}$

Expression of the spatial velocity potential in Region Ω_1 may be written as

$$\phi_1 = -\frac{igA}{\omega} e^{ikx} Z_0(\tilde{x}) + \sum_{n=0}^{\infty} A_n e^{-ik_n x} Z_n(\tilde{x}), \quad (14)$$

where the first term on its right-hand side represents the undisturbed incident spatial velocity potential, ϕ_I . A_n are the unknown coefficients to be determined. $k_0 = k \in \mathbb{R}^+$ and $k_n \in i\mathbb{R}^+$ for $n = 1, 2, \dots$ support the propagating waves and evanescent waves, respectively, and they are the positive real root and the infinite positive imaginary roots of the dispersion equation,

$$\frac{\omega^2}{g} = k_n \tanh(k_n b); \quad (15)$$

The corresponding depth functions $Z_n(\tilde{x})$ are expressed as

$$Z_n(\tilde{x}) = \frac{\cosh[k_n(\tilde{x} + b)]}{\cosh(k_n b)}. \quad (16)$$

Region Ω_4 $\{x \in [l_0, \infty), \tilde{x} \in [-b, 0]\}$

Expression of the spatial velocity potential in Region Ω_4 can be expressed as

$$\phi_4 = \sum_{n=0}^{\infty} B_n e^{ik_n x} Z_n(\tilde{x}), \quad (17)$$

where B_n are the unknown coefficients to be determined.

2.2.2 | Region $\Omega_2 \{z \in [-b, 0], x \in [-l, 0]\}$

In region Ω_2 , the potential may be written as

$$\phi_2(x, z) = \sum_{n=-2}^{\infty} (C_n e^{\kappa_n x} + D_n e^{-\kappa_n x}) Y_n(z), \quad (18)$$

where C_n and D_n are the unknown coefficients to be determined;

$$Y_n(z) = \begin{cases} -\sin(\kappa_n z) \left[\kappa_n b \cos(\kappa_n z) + \frac{\omega^2}{g} b \sin(\kappa_n z) \right], & \text{on } z \in [-d, 0] \\ \cos[\kappa_n(z+b)] \left[\kappa_n b \sin(\kappa_n d) + \frac{\omega^2}{g} b \cos(\kappa_n d) \right], & \text{on } z \in [-b, -d] \end{cases} \quad (19)$$

in which $c = b - d$; κ_n for $n = -2, -1, 0, 1, 2, \dots$ are the roots of the dispersion relation for the pWEC,

$$\begin{aligned} & \left[\chi \left(1 + \frac{\beta^2 \zeta \omega}{i + \zeta \omega} \right) \kappa^4 - \frac{\omega^2}{g} \gamma \right] \left[\kappa \sin(\kappa d) + \frac{\omega^2}{g} \cos(\kappa d) \right] \tan(\kappa c) \\ & = -\frac{\omega^2}{g} \left\{ \left[\cos(\kappa d) - \frac{\omega^2}{g \kappa} \sin(\kappa d) \right] \tan(\kappa c) + \sin(\kappa d) + \frac{\omega^2}{g \kappa} \cos(\kappa d) \right\}, \end{aligned} \quad (20)$$

which can be derived by inserting Equation (18) into Equation (11).

Particularly, if $\beta = 0$ or $\zeta = 0$, the plate turns into a submerged elastic plate, for which the corresponding properties of the roots can be found in [41]. Once the roots for $\beta = 0$ or $\zeta = 0$ are determined, the roots of the dispersion relation for $\beta \neq 0$ and $\zeta \neq 0$ can then be derived by using the homotopy method, starting with the corresponding roots for the case of $\beta = 0$ or $\zeta = 0$ [42, 43].

2.2.3 | Region $\Omega_3 \{x \in [0, l_0], z \in [-b, -d_0]\}$

The velocity potential in the fluid domain under the breakwater, that is Region Ω_3 can be expressed as

$$\phi_3(x, z) = E_0 x + F_0 + \sum_{n=1}^{\infty} (E_n e^{\beta_n x} + F_n e^{-\beta_n x}) \cos[\beta_n(z+b)], \quad (21)$$

where $\beta_n = \frac{n\pi}{b-d_0}$; E_n and F_n for $n = 0, 1, 2, \dots$ are the unknown coefficients to be determined.

2.3 | Continuity conditions

Continuity conditions at the interfaces of the adjacent regions and the side wall of the breakwater should be satisfied:

$$\phi_1|_{x=-l} = \phi_2|_{x=-l}, \quad z \in [-b, 0] \quad (22)$$

$$\phi_2|_{x=0} = \phi_3|_{x=0}, \quad z \in [-b, -d_0] \quad (23)$$

$$\phi_3|_{x=l_0} = \phi_4|_{x=l_0}, \quad z \in [-b, -d_0] \quad (24)$$

$$\partial_x \phi_1|_{x=-l} = \partial_x \phi_2|_{x=-l}, \quad z \in [-b, 0], \quad (25)$$

$$\partial_x \phi_2|_{x=0} = \begin{cases} 0, & z \in [-d_0, 0], \\ \partial_x \phi_3|_{x=0}, & z \in [-b, -d_0], \end{cases} \quad (26)$$

$$\partial_x \phi_4|_{x=l_0} = \begin{cases} 0, & z \in [-d_0, 0], \\ \partial_x \phi_3|_{x=l_0}, & z \in [-b, -d_0]. \end{cases} \quad (27)$$

These continuity conditions, together with the edge conditions, can form a linear algebraic system after truncation of the infinite series of vertical eigenfunctions at N , and can be further employed to determine the unknown coefficients A_n, B_n, C_n, D_n, E_n and F_n . The complicated deduction process of the formulas and calculation of these unknown coefficients are given in the Appendix.

2.4 | Free-surface elevation

The elevation of the air–water interface vertically deviating from the still water level, that is the free-surface elevation, is expressed as:

$$\eta_0(x) = \frac{i\omega}{g} \phi|_{z=0}. \quad (28)$$

2.5 | Plate displacement

The displacement of the pWEC about $z = -d$ can be calculated in terms of C_n and D_n as

$$\begin{aligned} \xi = \frac{i}{\omega} \partial_z \phi|_{z=-d} = & -\frac{i}{\omega} \sum_{n=-2}^{\infty} \kappa_n \sin(\kappa_n c) \left[\kappa_n b \sin(\kappa_n d) \right. \\ & \left. + \frac{\omega^2}{g} b \cos(\kappa_n d) \right] (C_n e^{\kappa_n x} + D_n e^{-\kappa_n x}). \end{aligned} \quad (29)$$

2.6 | Hydrodynamic force acting on the plate

The vertical hydrodynamic force acting on the plate can be calculated by integrating the hydrodynamic pressure drop across the pWEC over $x \in [-l, 0]$

$$\begin{aligned} F_e = i\omega\rho \int_{-l}^0 (\phi_- - \phi_+) |_{z=-d} dx \\ = i\omega\rho \sum_{n=-2}^{\infty} [C_n(1 - e^{-\kappa_n l}) - D_n(1 - e^{\kappa_n l})] \\ \times \left(b \sin(\kappa_n b) + \frac{\omega^2 b}{g \kappa_n} \cos(\kappa_n b) \right). \end{aligned} \quad (30)$$

2.7 | Wave reflection and transmission

The wave reflection and transmission coefficients denoted by R and T , respectively, can be calculated by

$$R = \frac{\omega}{gA} |A_0|, \quad T = \frac{\omega}{gA} |B_0|. \quad (31)$$

2.8 | Wave power absorption

2.8.1 | Direct method

Wave power absorption by the pWEC may be evaluated in a straightforward manner following [28, 35]

$$\begin{aligned} P_{\text{ext}} &= \frac{\omega^2 \rho g}{2} \frac{\beta^2 \chi \zeta}{1 + \omega^2 \zeta^2} \int_{-l}^0 |\partial_x^2 \xi|^2 dx \\ &= \frac{\rho g}{2} \frac{\beta^2 \chi \zeta}{1 + \omega^2 \zeta^2} \int_{-l}^0 |\partial_x^3 \phi|_{\zeta=-d}^2 dx, \\ &= \frac{\rho g}{2} \frac{\beta^2 \chi \zeta}{1 + \omega^2 \zeta^2} \left\{ \sum_{n=-2}^{\infty} \sum_{m=-2}^{\infty} \kappa_n^3 \kappa_m^{*3} \sin(\kappa_n c) \sin(\kappa_m^* c) \right. \\ &\quad \times \left[\kappa_n b \sin(\kappa_n d) + \frac{\omega^2}{g} b \cos(\kappa_n d) \right] \\ &\quad \times \left[\kappa_m^* b \sin(\kappa_m^* d) + \frac{\omega^2}{g} b \cos(\kappa_m^* d) \right] \\ &\quad \times \left[\frac{C_n C_m^* (1 - e^{-(\kappa_n + \kappa_m^*)l})}{\kappa_n + \kappa_m^*} - \frac{D_n D_m^* (1 - e^{(\kappa_n + \kappa_m^*)l})}{\kappa_n + \kappa_m^*} \right. \\ &\quad \left. \left. + \frac{C_n D_m^* (1 - e^{-(\kappa_n - \kappa_m^*)l})}{\kappa_n - \kappa_m^*} - \frac{C_m^* D_n (1 - e^{(\kappa_n - \kappa_m^*)l})}{\kappa_n - \kappa_m^*} \right] \right\}. \quad (32) \end{aligned}$$

We introduce the relative absorbed power, that is wave power absorption efficiency

$$\eta_{\text{ext}} = \frac{P_{\text{ext}}}{P_{\text{inc}}}, \quad (33)$$

where

$$P_{\text{inc}} = \frac{\rho g A^2}{2} \frac{\omega}{2k} \left(1 + \frac{2kb}{\sinh(2kb)} \right) \quad (34)$$

denotes the incoming wave power.

2.8.2 | Indirect method

Apart from the direct method, an indirect method can be derived based on Green's theorem

$$\begin{aligned} P_{\text{ext}} &= \frac{\rho \omega}{4i} \int_{-b}^0 \left[\left(\phi \frac{\partial \phi^*}{\partial x} - \phi^* \frac{\partial \phi}{\partial x} \right) \Big|_{x=X} \right. \\ &\quad \left. - \left(\phi \frac{\partial \phi^*}{\partial x} - \phi^* \frac{\partial \phi}{\partial x} \right) \Big|_{x=-X} \right] dz, \quad (35) \end{aligned}$$

where $X > \max\{l, l_0\}$. When $X \rightarrow \infty$, only propagating waves remain, and Equation (35) can be rewritten as

$$P_{\text{ext}} = \frac{\rho \omega [\sinh(kb) \cosh(kb) + kb]}{4 \cosh^2(kb)} \left(\frac{g^2 A^2}{\omega^2} - |A_0|^2 - |B_0|^2 \right), \quad (36)$$

resulting in the corresponding wave power absorption efficiency

$$\eta_{\text{ext}} = 1 - R^2 - T^2, \quad (37)$$

which is in line with the energy conservation, indicating the incident wave power is absorbed, reflected and transmitted by the breakwater integrated pWEC.

3 | CONVERGENCE ANALYSIS

Figure 2 illustrates the impact of the truncated cutoffs (i.e. in terms of N) on the frequency response of wave power absorption efficiency and wave transmission coefficient for a floating breakwater integrated pWEC with $l_0/b = 0.5$, $d_0/b = 0.5$, $l/b = 1.0$, $d/b = 0.2$, $\bar{\chi} = \chi/b^4 = 4.78 \times 10^{-7}$, $\bar{\gamma} = \gamma/b = 1.258 \times 10^{-3}$, $\beta = 0.24$ and $\bar{\zeta} = \zeta \sqrt{g/b} = 1.0$. In order to obtain the converged results, $N \geq 40$ is suggested. Hereinafter, $N = 40$ is adopted.

4 | MODEL VALIDATION

When $d_0/b = 1.0$ (or $d_0/b \rightarrow 1.0$), the bottom of the floating breakwater touches (or approaches) the sea bed, making the system become (or work similar to) a pWEC mooring in front of a bottom-seated breakwater, the hydrodynamic problem of which has already been numerically studied by Buriani & Renzi [35]. Moreover, if either χ or γ is large enough, the pWEC would work as a rigid plate, and the present hydrodynamic problem becomes the wave reflection by a vertical wall with a horizontal submerged rigid plate studied by Wu et al. [44]. Figure 3 presents a comparison of wave power absorption efficiency between the present results and those of [35]. Variation of the free-surface elevation at $x = 0$ and the vertical hydrodynamic force acting on the pWEC for $\bar{\chi} = \chi/b^4 = 10^4$ versus pWEC width, together with the corresponding published data associated with a rigid

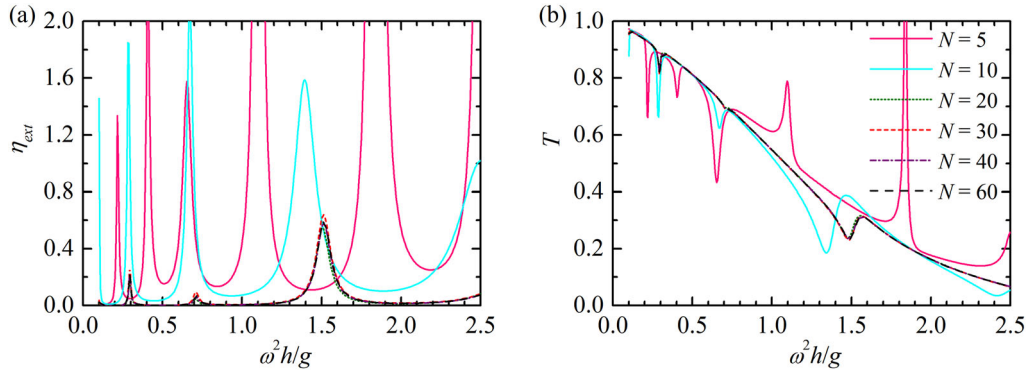


FIGURE 2 Impact of the truncated cut-offs (i.e. in terms of N) on wave power absorption and wave attenuation, $l_0/b = 0.5$, $d_0/b = 0.5$, $l/b = 1.0$, $d/b = 0.2$, $\bar{\chi} = \chi/b^4 = 4.78 \times 10^{-7}$, $\bar{\gamma} = \gamma/b = 1.258 \times 10^{-3}$, $\beta = 0.24$ and $\bar{\zeta} = \zeta\sqrt{g}/b = 1.0$: (a) η_{ext} ; (b) T .

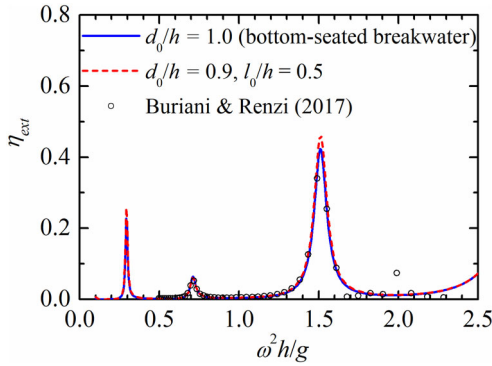


FIGURE 3 Frequency response of wave power absorption efficiency, $l/b = 1.0$, $d/b = 0.2$, $\bar{\chi} = \chi/b^4 = 4.78 \times 10^{-7}$, $\bar{\gamma} = \gamma/b = 1.258 \times 10^{-3}$, $\beta = 0.24$ and $\bar{\zeta} = \zeta\sqrt{g}/b = 1.0$

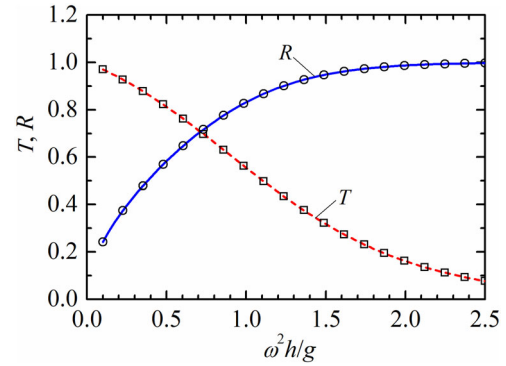


FIGURE 5 Frequency response of the wave transmission coefficient and reflection coefficient, $l_0/b = 0.5$, $d_0/b = 0.5$. Lines: present results with $l/b = 0.01$, $d/b = 0.2$, $\bar{\chi} = \chi/b^4 = 4.78 \times 10^{-7}$, $\bar{\gamma} = \gamma/b = 1.258 \times 10^{-3}$, $\beta = 0.24$ and $\bar{\zeta} = \zeta\sqrt{g}/b = 1.0$; Symbols: Zheng and Zhang [39]

plate placed in front of a vertical wall [44], are plotted in Figure 4.

If the width of the pWEC is small enough, the floating breakwater integrated pWEC is expected to work as a single breakwater. Figure 5 illustrates the comparison of the wave reflection/transmission coefficients of a floating breakwater integrated pWEC with $l_0/b = 0.5$, $d_0/b = 0.5$, $l/b = 0.01$, $d/b = 0.2$, and those of a single isolated breakwater [39].

In addition to the above three extreme circumstances, a more general case with $l_0/b = 0.5$, $d_0/b = 0.5$, $l/b = 1.0$, $d/b = 0.2$ is examined, the wave power absorption efficiency of which is calculated by using both the direct and indirect methods, and the comparison between them is illustrated in Figure 6.

The excellent agreement between the results shown in Figures 3–6 gives confidence in the present model for solving the

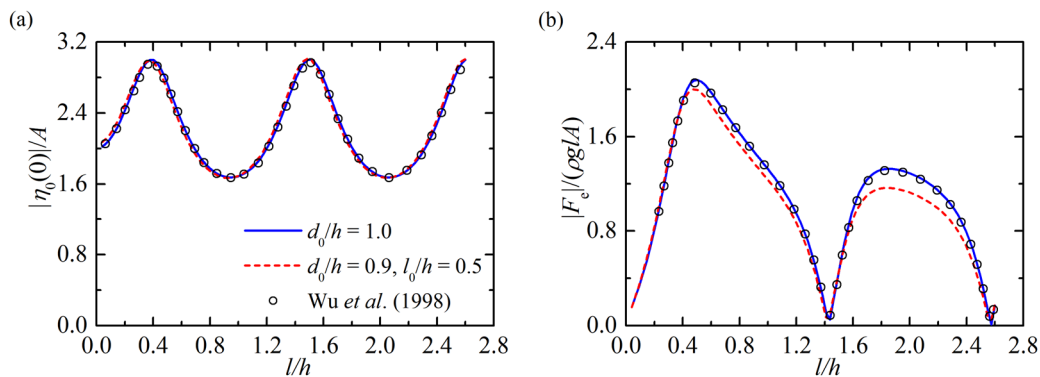


FIGURE 4 Variation of wave amplitude at $x = 0$ and the hydrodynamic wave force acting on the plate versus plate length, $\omega^2 b/g = 1.44$ (wavelength = $4.0b$), $d/b = 0.2$, $\bar{\chi} = \chi/b^4 = 10^{-4}$, $\bar{\gamma} = \gamma/b = 1.258 \times 10^{-3}$, $\beta = 0.24$ and $\bar{\zeta} = \zeta\sqrt{g}/b = 1.0$: (a) $|\eta_0|/A$; (b) $|F_c|/\rho g LA$

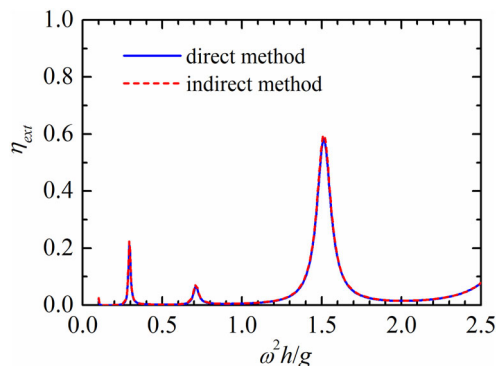


FIGURE 6 Frequency response of the wave power absorption efficiency, $l_0/b = 0.5$, $d_0/b = 0.5$, $l/b = 1.0$, $d/b = 0.2$, $\bar{\chi} = \chi/b^4 = 4.78 \times 10^{-7}$, $\bar{\gamma} = \gamma/b = 1.258 \times 10^{-3}$, $\beta = 0.24$ and $\bar{\xi} = \xi\sqrt{g/b} = 1.0$

problem of wave interaction with a floating breakwater integrated pWEC.

5 | RESULTS AND DISCUSSION

In this section, the validated model is adapted to study the effects of the pWEC width, pWEC submergence, breakwater width and breakwater draft, together with the type of the pWEC edge, on wave power absorption and wave attenuation of the floating breakwater integrated pWEC.

5.1 | Effect of the plate edge type

Figure 7 shows that the performance of the pWEC in terms of wave power absorption is dramatically influenced by the edge types. In the computed range of wave frequencies, that is $\omega^2 b/g \in [0.1, 2.5]$, there are three and four peaks of the $\eta_{ext} - \omega^2 b/g$ curves observed for the clamped and simply supported edge conditions, respectively. For the clamped edge condition, the peak values of η_{ext} and the corresponding $\omega^2 b/g$

are (0.22,0.29), (0.07,0.71) and (0.58,1.51). Correspondingly, for the simply supported edge conditions, they are (0.06,0.20), (0.01,0.51), (0.28,1.14) and (0.57,2.26).

This may be explained from the point of view of resonance. The more strictly the plate edge is constrained, the larger the stiffness of the plate, resulting in larger wave frequencies where the peaks occur.

The transmission coefficient presents an overall decreasing trend with increase of the wave frequency (Figure 7(b)). Several sudden drops of T are observed at the frequencies where the peaks of η_{ext} happen.

Figure 8 presents a snapshot of the system with the displacements of the pWEC and the free-surface elevation at the seaside and leeward of the breakwater. The incident water waves have amplitude $A = 0.2$ m and period of 5 s, corresponding to a wavelength of 36.58 m. The free surface is found to match seamlessly across Regions Ω_1 and Ω_{2a} defined in subsection 2.2 (Figure 1(b)). The clamping (i.e. Equation 13) and simply supported (i.e. Equation 12) edge conditions are correctly satisfied by the analytical solutions. On the plate, short-crested oscillations are created by a short, weakly damped progressive wave, which has also been reported by Renzi [28] for an offshore stand-alone pWEC. This can be explained from the properties of the root of the dispersion equation for the pWEC. Due to the coupled hydroelectromechanical effect, a coupled system of long- and short-crested weakly damped flexural waves with the length of 36.56 m and 2.72 m, which correspond to the roots $\kappa_0 = (-7.73 \times 10^{-9} + 1.72 \times 10^{-1}i)$ m^{-1} and $\kappa_1 = (-1.25 \times 10^{-2} + 2.31i)$ m^{-1} , respectively, are excited by the incident waves. For the present case, the short-crested weakly damped flexural wave dominates the plate displacements.

5.2 | Effect of the plate width, l

Figure 9 plots the wave power absorption efficiency and wave transmission coefficient of the floating breakwater integrated pWEC against $\omega^2 b/g$ for different values of pWEC width in terms of l/b . In the computed range of wave frequencies,

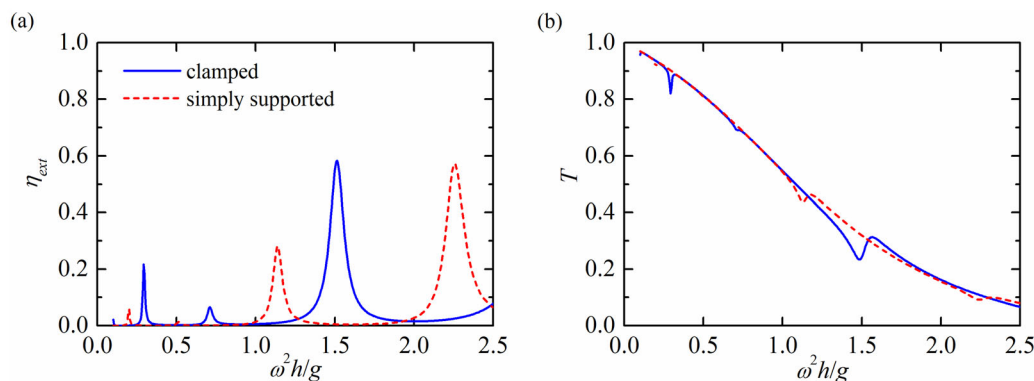


FIGURE 7 Frequency response of the wave power absorption efficiency and wave transmission coefficient for different edge conditions, $l_0/b = 0.5$, $d_0/b = 0.5$, $l/b = 1.0$, $d/b = 0.2$, $\bar{\chi} = \chi/b^4 = 4.78 \times 10^{-7}$, $\bar{\gamma} = \gamma/b = 1.258 \times 10^{-3}$, $\beta = 0.24$ and $\bar{\xi} = \xi\sqrt{g/b} = 1.0$: (a) η_{ext} ; (b) T

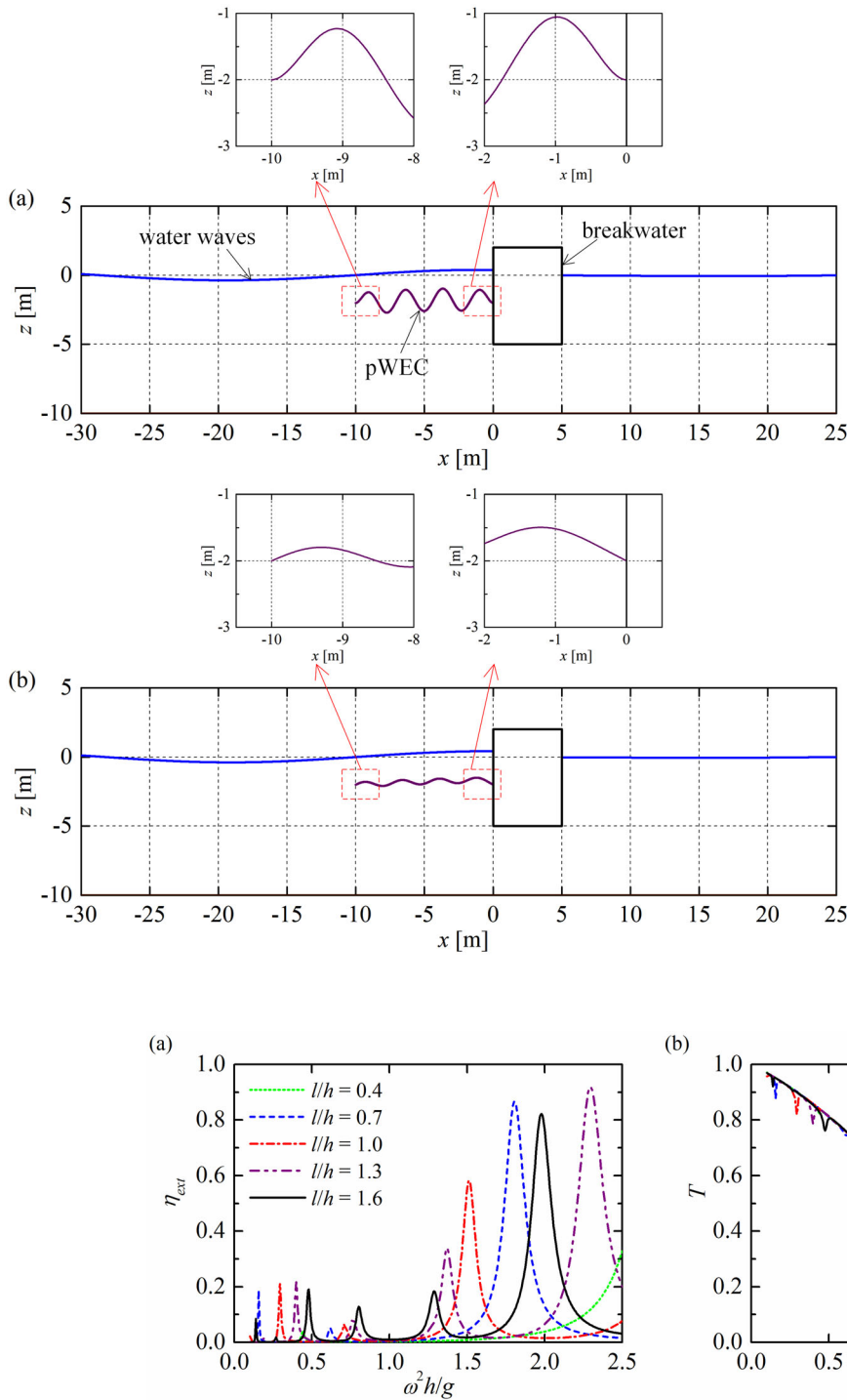


FIGURE 8 Snapshot of the free-surface elevation and plate displacement at $t = 0$, $A = 0.2$ m, $b = 10$ m, $\omega^2 b/g = 1.61$ (wave period = 5 s), $l_0/b = 0.5$, $d_0/b = 0.5$, $l/b = 1.0$, $d/b = 0.2$, $\bar{\chi} = \chi/b^4 = 4.78 \times 10^{-7}$, $\bar{\gamma} = \gamma/b = 1.258 \times 10^{-3}$, $\beta = 0.24$ and $\bar{\zeta} = \zeta \sqrt{g/b} = 1.0$: (a) clamped edge; (b) simply supported edge.

the larger the width of the pWEC, the more peaks of the $\eta_{ext} - \omega^2 b/g$ are observed. This can be explained from the view of the natural vibration frequencies of a beam with fixed ends and distributed mass, which are proportional to l^{-2} .

For most of the cases studied, the larger the wave frequencies where the peaks of the $\eta_{ext} - \omega^2 b/g$ occur, the larger the peaks in terms of both the peak value and bandwidth are observed. It

is noted that $\eta_{ext} > 0.8$ can be achieved at specified wave frequencies for the cases with $l/b = 0.7, 1.3$ and 1.6 .

Unlike the wave power absorption efficiency (Figure 9(a)), the wave transmission coefficients plotted in Figure 9(b) are found to be rather insensitive to the change of pWEC width, unless the peaks of η_{ext} occur, making the $T - \omega^2 b/g$ curves present a local inverted 'N' shape.

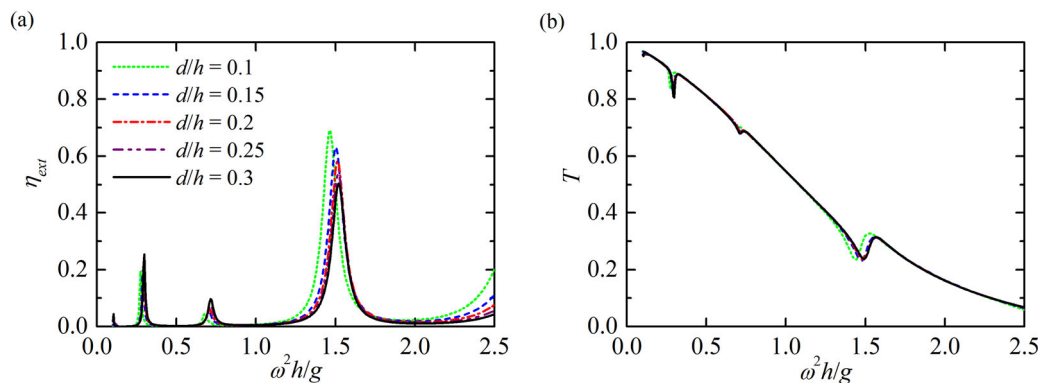


FIGURE 10 Frequency response of the wave power absorption efficiency and wave transmission coefficient for different plate submergence, $l_0/b = 0.5$, $d_0/b = 0.5$, $l/b = 1.0$, $\bar{\chi} = \chi/b^4 = 4.78 \times 10^{-7}$, $\bar{\gamma} = \gamma/b = 1.258 \times 10^{-3}$, $\beta = 0.24$ and $\bar{\xi} = \xi \sqrt{g/b} = 1.0$: (a) η_{ext} ; (b) T

The integrated system has a dual-function of wave power absorption and wave attenuation. The effective frequency bandwidth simultaneously satisfied with the requested absorption efficiency and transmission coefficient may be of interest. In the computed range of wave frequencies, the non-dimensional frequency bandwidths with $\eta_{ext} > 0.3$ and $T < 0.3$ are 0.01 ([2.49, 2.50]), 0.20 ([1.71, 1.91]), 0.07 ([1.47, 1.53]), 0.27 ([2.17, 2.44]) and 0.20 ([1.88, 2.09]) for $l/b = 0.4, 0.7, 1.0, 1.3$ and 1.6 , respectively. Hence, from the perspective of the effective dual-function, the $l/b = 1.3$ case may be the most promising among the five cases examined.

5.3 | Effect of the plate submergence, d

The submergence of the plate is one of the key parameters affecting the roots of the dispersion equation for the pWEC (see Equation 20), and is expected to influence the hydroelasticity of the pWEC further. The system with $d/b = 0.1, 0.15, 0.2, 0.25$ and 0.3 are selected as five cases to examine the effect of the pWEC submergence on wave power absorption and wave attenuation (Figure 10).

As indicated in Figure 10(a), as d/b increases, the main peaks of η_{ext} around $\omega^2 b/g = 1.5$ become lower and narrower. This could be because most wave power is concentrated at less than one-quarter of a wavelength below the water level, and the kinetic energy at a deeper position is less intensive than that at a shallower position. However, it should be noted that the other two peaks located at $\omega^2 b/g \approx 0.3$ and 0.7 (corresponding to the wavelength of 108.96 and 66.31 m, respectively) become higher with the increase of d/b . For these wave conditions, the wavelength is long enough that the kinetic energy is almost independent of the vertical position in the fluid domain, and does not dominate wave power absorption of the pWEC anymore.

With the increase of d/b , the peaks of η_{ext} shift towards high wave frequencies, and this may be explained from the view of added-mass, which increases as d/b becomes larger [45], resulting in larger natural resonant frequencies.

The wave transmission coefficient as plotted in Figure 10(b) is found to be insensitive to the change of the pWEC submergence.

5.4 | Effect of the breakwater width, l_0

The effect of the breakwater width on wave power absorption and wave attenuation is illustrated in Figure 11. As expected, the $T - \omega^2 b/g$ curves descend along with the raise of breakwater width (Figure 11(b)). It is also expected that when the breakwater is wide enough, it will work like a bottom-seated breakwater and that no wave power will be transmitted to its leeside.

In contrast to the change of the breakwater width on wave attenuation, its influence on wave power absorption of the pWEC is found to be rather limited (Figure 11(a)). As l_0/b increases from 0.1 to 0.9, the peak value of η_{ext} around $\omega^2 b/g = 1.5$ decreases merely by 11.6% from 0.62 to 0.55. It should be emphasised that this is a ‘decrease’ change of η_{ext} , although not too much, instead of ‘increase’, meaning that enlarging the breakwater width not only weakens wave attenuation but also suppresses wave power absorption of the pWEC.

5.5 | Effect of the breakwater draft, d_0

The effect of varying the breakwater draft on wave absorption and wave attenuation is also investigated by examining five cases with d_0/b ranging from 0.3 to 0.7 with a step of 0.1 (Figure 12).

As demonstrated in Figure 12, the variation of d_0/b plays a similar role as that of the breakwater width l_0/b on the performance of the floating breakwater integrated pWEC as plotted in Figure 11, but in a more dramatic manner. More specifically, as d_0/b increases from 0.3 to 0.7, the main peak value of η_{ext} drops from 0.66 to 0.52 by 21.7%. Moreover, the bandwidth of the main peak is compressed.

For $d_0/b = 1.0$, $\partial_x \phi = 0$, that is null horizontal fluid velocity, should be satisfied at $x = 0$ all over the water depth, that is the fluid particles below the pWEC are not allowed to pass through

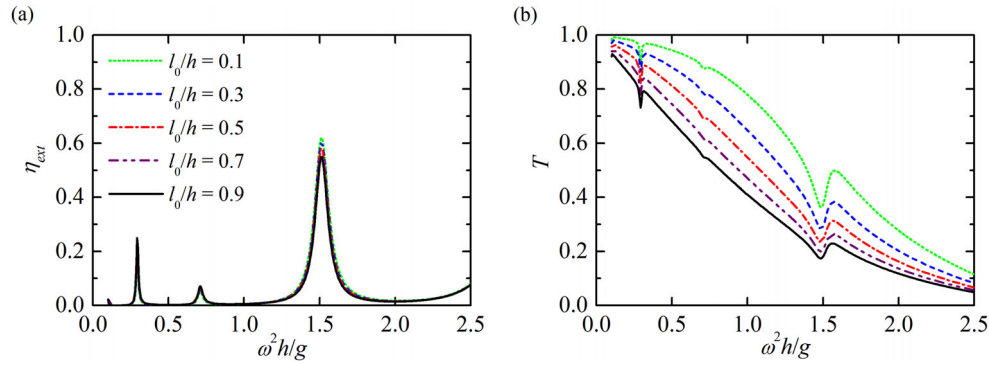


FIGURE 11 Frequency response of the wave power absorption efficiency and wave transmission coefficient for different breakwater widths, $d_0/b = 0.5$, $l/b = 1.0$, $d/b = 0.2$, $\bar{\chi} = \chi/b^4 = 4.78 \times 10^{-7}$, $\bar{\gamma} = \gamma/b = 1.258 \times 10^{-3}$, $\beta = 0.24$ and $\bar{\zeta} = \zeta\sqrt{g}/b = 1.0$: (a) η_{ext} ; (b) T

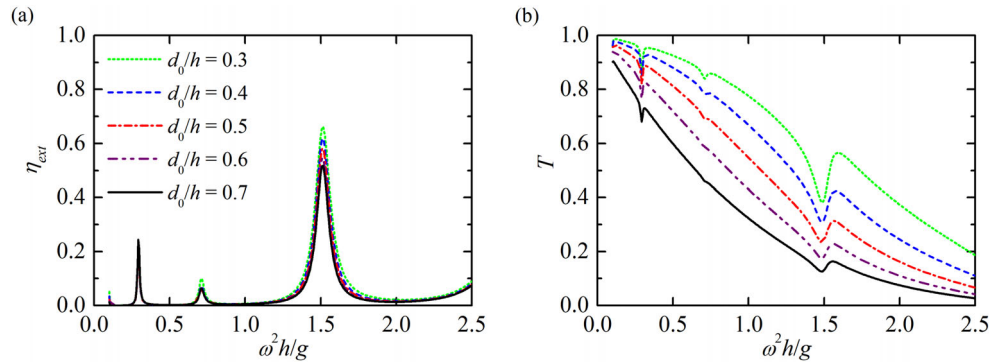


FIGURE 12 Frequency response of the wave power absorption efficiency and wave transmission coefficient for different breakwater drafts, $l_0/b = 0.5$, $l/b = 1.0$, $d/b = 0.2$, $\bar{\chi} = \chi/b^4 = 4.78 \times 10^{-7}$, $\bar{\gamma} = \gamma/b = 1.258 \times 10^{-3}$, $\beta = 0.24$ and $\bar{\zeta} = \zeta\sqrt{g}/b = 1.0$: (a) η_{ext} ; (b) T

the plane of $x = 0$. As a comparison, for $d_0/b < 1.0$, the fluid particles under the pWEC are free to move across $x = 0$ for $z \in [-b, -d_0]$, which may further liberate the motion of the pWEC and ultimately enhance wave power absorption.

6 | CONCLUSIONS

This paper considers a pWEC moored in front of a floating breakwater. The pWEC consists of a submerged flexible plate with piezoelectric layers bonded to both faces of it. The elastic motion of the plate can be transformed into useful electricity due to the piezoelectric effect. To evaluate the performance of the system, a 2D theoretical model is proposed based on linear potential flow theory and the eigenfunction matching method coupling the electromechanical and the hydrodynamic problems.

The theoretical model was first validated by comparing the present results with published data for different extreme cases, and an excellent agreement between them was achieved. The validated model was ultimately applied to explore the influence of the edge condition, width and submergence of the pWEC and the width and draft of the breakwater on wave power absorption and wave attenuation. The following conclusions may be drawn:

1. Wave power absorption of the pWEC is dramatically influenced by the edge types. There are three and four peaks of the $\eta_{ext} - \omega^2 h/g$ curves in the computed range of wave frequencies for the clamped and simply supported edge conditions, respectively.
2. As the width of the pWEC increases, more peaks of the $\eta_{ext} - \omega^2 h/g$ curves can be excited. As pWEC moves towards a deeper position, the main peaks of η_{ext} around $\omega^2 h/g = 1.5$ become lower and narrower. Varying the width or submergence of the pWEC, the influence on wave attenuation of the system is limited.
3. Wave transmission coefficient can be effectively reduced all over the examined wave frequencies by increasing either the width or the draft of the breakwater. Nevertheless, the change of the breakwater width/draft has limited influence on wave power absorption of the pWEC.

The present work is focused on the hydroelastic problem of a breakwater integrated pWEC with a fixed distributed-parameter model of the piezoelectric system adopted from [28, 35]. The device's wave power absorption could be enhanced if the piezoelectric system can be appropriately selected and optimised. The breakwater was assumed to be stationary, and its oscillation was not registered in our present model. However, this is an aspect of interest that we plan to investigate as a continuation

of this line of research. How to broaden the effective frequency bandwidth for such an integrated system is also an interesting research topic for future work.

ACKNOWLEDGEMENTS

The research was supported by Open Research Fund Program of State key Laboratory of Hydrosience and Engineering (Tsinghua University) (grant no. sklhse-2021-E-02) and Open Research Fund Program of State Key Laboratory of Ocean Engineering (Shanghai Jiao Tong University) (grant no. 1916). S. Zheng was supported by the European Union funded Marine-I (2nd phase) project (grant no. 05R18P02816). Zheng wishes to thank Prof. Bin Teng from Dalian University of Technology for valuable discussions. X. Zhang was supported by the 2020 Research Program of Sanya Yazhou Bay Science and Technology City (grant no. SKJC-2020-01-006) and Hainan Provincial Natural Science Foundation of China (grant no. 520QN290)

ORCID

Siming Zheng  <https://orcid.org/0000-0001-7124-1619>

Xiantao Zhang  <https://orcid.org/0000-0002-3795-3556>

REFERENCES

- Clément, A., et al.: Wave energy in Europe: Current status and perspectives. *Renewable Sustainable Energy Rev.* 6(5), 405–431 (2002)
- Drew, B., Plummer, A.R., Sahinkaya, M.N.: A review of wave energy converter technology. *Proc. Inst. Mech. Eng. Part A-J. Power Energy* 223(A8), 887–902 (2009)
- Mustapa, M.A., et al.: Wave energy device and breakwater integration: A review. *Renewable Sustainable Energy Rev.* 77, 43–58 (2017)
- Zhang, H., et al.: Hydrodynamic performance of a floating breakwater as an oscillating-buoy type wave energy converter. *Appl. Energy* 257, 113996 (2020)
- Evans, D.V., Porter, R.: Hydrodynamic characteristics of an oscillating water column device. *Appl. Ocean Res.* 17(3), 155–164 (1995)
- Martins-rivas, H., Mei, C.C.: Wave power extraction from an oscillating water column along a straight coast. *Ocean Eng.* 36(6-7), 426–433 (2009)
- Zheng, S., Zhang, Y., Iglesias, G.: Coast/breakwater-integrated OWC: A theoretical model. *Mar. Struct.* 66, 121–135 (2019)
- Zheng, S., et al.: Wave power extraction from multiple oscillating water columns along a straight coast. *J. Fluid Mech.* 878, 445–480 (2019)
- He, F., et al.: Hydrodynamic performance of a pile-supported OWC breakwater: An analytical study. *Appl. Ocean Res.* 88, 326–340 (2019)
- Morris-Thomas, M.T., Irvin, R.J., Thiagarajan, K.P.: An investigation into the hydrodynamic efficiency of an oscillating water column. *J. Offshore Mech. Arct. Eng.* 129(4), 273–278 (2007)
- López, I., Iglesias, G.: Efficiency of OWC wave energy converters: A virtual laboratory. *Appl. Ocean Res.* 4, 63–70 (2014)
- Falcão, A.F.D.O., Henriques, J.C.C., Gato, L.M.C.: Air turbine optimization for a bottom-standing oscillating-water-column wave energy converter. *J. Ocean Eng. Mar. Energy* 2(4), 459–472 (2016)
- He, F., Leng, J., Zhao, X.: An experimental investigation into the wave power extraction of a floating box-type breakwater with dual pneumatic chambers. *Appl. Ocean Res.* 67, 21–30 (2017)
- Pawitan, K.A., et al.: Front wall and in-chamber impact loads on a breakwater-integrated oscillating water column. *J. Waterw. Port Coastal Ocean Eng.* 146(5), 04020037 (2020)
- Zheng, S., et al.: Wave power extraction from a tubular structure integrated oscillating water column. *Renewable Energy* 150, 342–355 (2020)
- Liu, Z., Xu, C., Kim, K.: Overall performance of a model owc system under the free-spinning mode: An experimental study. *Ocean Eng.* 227, 108890 (2021)
- Vicinanza, D., et al.: Innovative rubble mound breakwaters for overtopping wave energy conversion. *Coastal Eng.* 88, 154–170 (2014)
- Contestabile, P., et al.: Wave loadings acting on innovative rubble mound breakwater for overtopping wave energy conversion. *Coastal Eng.* 122, 60–74 (2017)
- Musa, M.A., et al.: Numerical simulation of wave flow over the overtopping breakwater for energy conversion (OBREC) device. *Procedia Eng.* 194, 166–173 (2017)
- Di Lauro, E., et al.: Advantages of an innovative vertical breakwater with an overtopping wave energy converter. *Coastal Eng.* 159, 103713 (2020)
- Contestabile, P., et al.: Overtopping breakwater for wave energy conversion: Review of state of art, recent advancements and what lies ahead. *Renewable Energy* 147, 705–718 (2020)
- Schay, J., Bhattacharjee, J., Guedes Soares, C.: Numerical modelling of a heaving point absorber in front of a vertical wall. In: *ASME 2013 32nd International Conference on Ocean, Offshore and Arctic Engineering*, Nantes (2013)
- Ning, D., et al.: Hydrodynamic performance of a pile-restrained wec-type floating breakwater: An experimental study. *Renewable Energy* 95, 531–541 (2016)
- Ning, D.Z., et al.: Hydrodynamic performance of an array of wave energy converters integrated with a pontoon-type breakwater. *Energies* 11(3) (2018)
- Zhao, X.L., Ning, D.Z., Liang, D.F.: Experimental investigation on hydrodynamic performance of a breakwater-integrated WEC system. *Ocean Eng.* 171, 25–32 (2019)
- Konispoliatis, D.N., Mavrakos, S.A.: Wave power absorption by arrays of wave energy converters in front of a vertical breakwater: A theoretical study. *Energies* 13(8), 1985 (2020)
- Zhang, C., Ning, D.: Hydrodynamic study of a novel breakwater with parabolic openings for wave energy harvest. *Ocean Eng.* 182, 540–551 (2019)
- Renzi, E.: Hydroelectromechanical modelling of a piezoelectric wave energy converter. *Proc. Roy. Soc. A: Math., Phys. Eng. Sci.* 472, 20160715 (2016)
- Farley, F.J.M., Rainey, R.C.T., Chaplin, J.R.: Rubber tubes in the sea. *Philos. Trans. R. Soc. London, Ser. A* 370(1959), 381–402 (2012)
- Zheng, S., et al.: Hydroelastic interaction between water waves and an array of circular floating porous elastic plates. *J. Fluid Mech.* 900, A20 (2020)
- Zheng, S., et al.: Water-wave interaction with submerged porous elastic disks. *Phys. Fluids* 32(4), 047106 (2020)
- Behera, H., Sahoo, T.: Hydroelastic analysis of gravity wave interaction with submerged horizontal flexible porous plate. *J. Fluids Struct.* 54, 643–660 (2015)
- Selvan, S.A., Behera, H.: Wave energy dissipation by a floating circular flexible porous membrane in single and two-layer fluids. *Ocean Eng.* 206, 107374 (2020)
- Zheng, S., et al.: Wave power extraction by a submerged piezoelectric plate. In: *Developments in Renewable Energies Offshore: Proceedings of the 4th International Conference on Renewable Energies Offshore*, Lisbon (2020)
- Buriani, F., Renzi, E.: Hydrodynamics of a flexible piezoelectric wave energy harvester moored on a breakwater. In: *12th European Wave and Tidal Energy Conference (EWTEC)*, Cork (2017)
- Athanassoulis, G.A., Mamis, K.I.: Modeling and analysis of a cliff-mounted piezoelectric sea-wave energy absorption system. *Coupled Syst. Mech.* 2(1), 53–83 (2013)
- Liu, C., Huang, Z.: A flexible membrane breakwater with a piezoelectric layer for providing harborage and wave-energy conversion. *J. Coastal Res.* 36(1), 148–156 (2019)
- Buriani, F.: Mathematical modelling of wave–structure interactions with application to wave energy conversion. *Dissertation*, Loughborough University (2019)
- Zheng, S., Zhang, Y.: Wave diffraction and radiation by multiple rectangular floaters. *J. Hydraul. Res.* 54(1), 102–115 (2016)

40. Zheng, S., Zhang, Y.: Analytical study on wave power extraction from a hybrid wave energy converter. *Ocean Eng.* 165, 252–263 (2018)
41. Mahmood-Ul-Hassan, M., Meylan, M.H., Peter, M.A.: Water-wave scattering by submerged elastic plates. *Q. J. Mech. Appl. Math.* 62(3), 321–344 (2009)
42. Meylan, M.H., Bennetts, L.G., Peter, M.A.: Water-wave scattering and energy dissipation by a floating porous elastic plate in three dimensions. *Wave Motion* 70, 240–250 (2017)
43. Zheng, S., et al.: Wave scattering by a floating porous elastic plate of arbitrary shape: a semi-analytical study. *J. Fluids Struct.* 92, 102827 (2020)
44. Wu, J., Wan, Z., Fang, Y.: Wave reflection by a vertical wall with a horizontal submerged porous plate. *Ocean Eng.* 25(9), 767–779 (1998)
45. Farina, L., et al.: Radiation of water waves by a submerged nearly circular plate. *J. Comput. Appl. Math.* 310, 165–173 (2017)

How to cite this article: Zheng, S., et al.: Performance of a plate-wave energy converter integrated in a floating breakwater. *IET Renew. Power Gener.* 15, 3206–3219 (2021). <https://doi.org/10.1049/rpg2.12230>

APPENDIX A

A.1 | Appendix derivation process of the formulas and calculation for the unknown coefficients A_n , B_n , C_n , D_n , E_n AND F_n

Here we take the case with simply supported edge condition as an example to show how to determine the unknown coefficients A_n , B_n , C_n , D_n , E_n and F_n . Inserting the expression of the spatial potentials at different regions of the fluid domain, that is Equations (14), (17), (18) and (21), into the continuity conditions, which should be satisfied at the interfaces between each two adjacent regions, and the simply supported edge boundary conditions, that is Equations (22)–(27) and (12), gives:

$$-\frac{igA}{\omega} e^{-ikl} Z_0(\zeta) + \sum_{n=0}^{\infty} A_n e^{ik_n l} Z_n(\zeta) = \sum_{n=-2}^{\infty} (C_n e^{-\kappa_n l} + D_n e^{\kappa_n l}) Y_n(\zeta), \quad \zeta \in [-b, 0], \quad (\text{A.1})$$

$$\sum_{n=-2}^{\infty} (C_n + D_n) Y_n(\zeta) = F_0 + \sum_{n=1}^{\infty} (E_n + F_n) \times \cos[\beta_n(\zeta + b)], \quad \zeta \in [-b, -d_0], \quad (\text{A.2})$$

$$E_0 l_0 + F_0 + \sum_{n=1}^{\infty} (E_n e^{\beta_n l_0} + F_n e^{-\beta_n l_0}) \times \cos[\beta_n(\zeta + b)] = \sum_{n=0}^{\infty} B_n e^{ik_n l_0} Z_n(\zeta), \quad \zeta \in [-b, -d_0], \quad (\text{A.3})$$

$$\frac{k_g A}{\omega} e^{-ikl} Z_0(\zeta) - i \sum_{n=0}^{\infty} k_n A_n e^{ik_n l} Z_n(\zeta)$$

$$= \sum_{n=-2}^{\infty} \kappa_n (C_n e^{-\kappa_n l} - D_n e^{\kappa_n l}) Y_n(\zeta), \quad \zeta \in [-b, 0], \quad (\text{A.4})$$

$$\sum_{n=-2}^{\infty} \kappa_n (C_n - D_n) Y_n(\zeta) = \begin{cases} 0, & \zeta \in [-d_0, 0], \\ E_0 + \sum_{n=1}^{\infty} \beta_n (E_n - F_n) \cos[\beta_n(\zeta + b)], & \zeta \in [-b, -d_0]. \end{cases} \quad (\text{A.5})$$

$$i \sum_{n=0}^{\infty} k_n B_n e^{ik_n l_0} Z_n(\zeta) = \begin{cases} 0, & \zeta \in [-d_0, 0], \\ E_0 + \sum_{n=1}^{\infty} \beta_n (E_n e^{\beta_n l_0} - F_n e^{-\beta_n l_0}) \cos[\beta_n(\zeta + b)], & \zeta \in [-b, -d_0]. \end{cases} \quad (\text{A.6})$$

$$\sum_{n=-2}^{\infty} \kappa_n \sin(\kappa_n c) \left[\kappa_n b \sin(\kappa_n d) + \frac{\omega^2}{g} b \cos(\kappa_n d) \right] \times (C_n e^{-\kappa_n l} + D_n e^{\kappa_n l}) = 0, \quad (\text{A.7})$$

$$\sum_{n=-2}^{\infty} \kappa_n \sin(\kappa_n c) \left[\kappa_n b \sin(\kappa_n d) + \frac{\omega^2}{g} b \cos(\kappa_n d) \right] \times (C_n + D_n) = 0, \quad (\text{A.8})$$

$$\sum_{n=-2}^{\infty} \kappa_n^3 \sin(\kappa_n c) \left[\kappa_n b \sin(\kappa_n d) + \frac{\omega^2}{g} b \cos(\kappa_n d) \right] \times (C_n e^{-\kappa_n l} + D_n e^{\kappa_n l}) = 0, \quad (\text{A.9})$$

$$\sum_{n=-2}^{\infty} \kappa_n^3 \sin(\kappa_n c) \left[\kappa_n b \sin(\kappa_n d) + \frac{\omega^2}{g} b \cos(\kappa_n d) \right] \times (C_n + D_n) = 0. \quad (\text{A.10})$$

If the plate is clamped at its edge, then Equations (A.9) and (A.10) should be replaced by

$$\sum_{n=-2}^{\infty} \kappa_n^2 \sin(\kappa_n c) \left[\kappa_n b \sin(\kappa_n d) + \frac{\omega^2}{g} b \cos(\kappa_n d) \right] \times (C_n e^{-\kappa_n l} - D_n e^{\kappa_n l}) = 0, \quad (\text{A.11})$$

and

$$\sum_{n=-2}^{\infty} \kappa_n^2 \sin(\kappa_n c) \left[\kappa_n b \sin(\kappa_n d) + \frac{\omega^2}{g} b \cos(\kappa_n d) \right] \times (C_n - D_n) = 0. \quad (\text{A.12})$$

The orthonormal properties of $Z_n(\zeta)$ and $\cos[\beta_n(\zeta + b)]$ can be used to help determine the unknown coefficients. Table A.1

TABLE A.1 Multiplying terms and the corresponding intervals of integration for Equations (A.1)–(A.6)

Equation	(A.1)	(A.2)	(A.3)	(A.4)	(A.5)	(A.6)
multiplying term	$Z_\tau(\tilde{z})$	$\cos[\beta_\tau(\tilde{z} + b)]$	$\cos[\beta_\tau(\tilde{z} + b)]$	$Z_\tau(\tilde{z})$	$Z_\tau(\tilde{z})$	$Z_\tau(\tilde{z})$
interval of integration	$[-b, 0]$	$[-b, -d_0]$	$[-b, -d_0]$	$[-b, 0]$	$[-b, 0]$	$[-b, 0]$

lists the multiplying terms and the corresponding intervals of integration for Equations (A.1)–(A.6).

After multiplying both sides of each equation among Equations (A.1)–(A.6) with the corresponding listed term, integrating vertically over the listed interval, and making some rearrangement, Equations (A.1)–(A.6) can be rewritten as

$$A_\tau e^{ik_\tau l} H_\tau^{(1)} - \sum_{n=-2}^{\infty} (C_n e^{-\kappa_n l} + D_n e^{\kappa_n l}) J_{n,\tau}^{(1)} = \delta_{0,\tau} \frac{igA}{\omega} e^{-ikl} H_0^{(1)}, \quad (A.13)$$

$$\sum_{n=-2}^{\infty} (C_n + D_n) J_{n,\tau}^{(2)} - \delta_{0,\tau} F_0 H_\tau^{(2)} - (1 - \delta_{0,\tau})(E_\tau + F_\tau) H_\tau^{(2)} = 0, \quad (A.14)$$

$$\sum_{n=0}^{\infty} B_n e^{ik_n l_0} J_{n,\tau}^{(3)} - \delta_{0,\tau}(E_0 l_0 + F_0) H_\tau^{(2)} - (1 - \delta_{0,\tau})(E_\tau e^{\beta_\tau l_0} + F_\tau e^{-\beta_\tau l_0}) H_\tau^{(2)} = 0, \quad (A.15)$$

$$ik_\tau A_\tau e^{ik_\tau l} H_\tau^{(1)} + \sum_{n=-2}^{\infty} \kappa_n (C_n e^{-\kappa_n l} - D_n e^{\kappa_n l}) J_{n,\tau}^{(1)} = \delta_{0,\tau} \frac{k_g A}{\omega} e^{-ikl} H_0^{(1)}, \quad (A.16)$$

$$\sum_{n=-2}^{\infty} \kappa_n (C_n - D_n) J_{n,\tau}^{(1)} - E_0 J_{\tau,0}^{(3)} - \sum_{n=1}^{\infty} \beta_n (E_n - F_n) J_{\tau,n}^{(3)} = 0, \quad (A.17)$$

$$ik_\tau B_\tau e^{ik_\tau l_0} H_\tau^{(1)} - E_0 J_{\tau,0}^{(3)} - \sum_{n=1}^{\infty} \beta_n (E_n e^{\beta_n l_0} - F_n e^{-\beta_n l_0}) J_{\tau,n}^{(3)} = 0, \quad (A.18)$$

where

$$H_n^{(1)} = \int_{-b}^0 Z_n^2(\tilde{z}) d\tilde{z} = \frac{\sinh(k_n b) \cosh(k_n b) + k_l b}{2k_n \cosh^2(k_n b)}, \quad (A.19)$$

$$H_n^{(2)} = \int_{-b}^{-d_0} \cos^2[\beta_n(\tilde{z} + b)] d\tilde{z} = \begin{cases} b - d_0, & n = 0 \\ \frac{b-d_0}{2}, & n = 1, 2, \dots \end{cases}, \quad (A.20)$$

$$J_{n,\tau}^{(1)} = \int_{-b}^0 Y_n(\tilde{z}) Z_\tau(\tilde{z}) d\tilde{z} = \frac{k_\tau b \sinh(k_\tau l) \left[\frac{\omega^2}{g} \cos(\kappa_n b) + \kappa_n \sin(\kappa_n b) \right]}{\cosh(k_\tau b) (\kappa_n^2 + k_\tau^2)}, \quad (A.21)$$

$$J_{n,\tau}^{(2)} = \int_{-b}^{-d_0} Y_n(\tilde{z}) \cos[\beta_\tau(\tilde{z} + b)] d\tilde{z} = \left[\kappa_n b \sin(\kappa_n d) + \frac{\omega^2 b}{g} \cos(\kappa_n d) \right] \times \frac{\kappa_n (b - d_0)^2 (-1)^\tau \sin[\kappa_n (b - d_0)]}{(b - d_0)^2 \kappa_n^2 - \tau^2 \pi^2}, \quad (A.22)$$

$$J_{n,\tau}^{(3)} = \int_{-b}^{-d_0} Z_n(\tilde{z}) \cos[\beta_\tau(\tilde{z} + b)] d\tilde{z} = \frac{(b - d_0)^2 (-1)^\tau k_n \sinh[k_n (b - d_0)]}{[(b - d_0)^2 k_n^2 + \tau^2 \pi^2] \cosh(k_n b)}. \quad (A.23)$$

To evaluate the unknown coefficients A_n, B_n, C_n, D_n, E_n and F_n , we truncate all infinite series of vertical eigenfunctions at N , that is $(N + 1)$ terms ($n = 0, 1, \dots, N$) for A_n, B_n, E_n and F_n and $(N + 3)$ terms ($n = -2, -1, 0, 1, \dots, N$) for C_n and D_n , resulting in $(6N + 10)$ unknown coefficients to be determined. After taking $(\tau = 0, 1, \dots, N)$ in Equations (A.13)–(A.18) and with the simply supported edge conditions Equations (A.7)–(A.10) appended, a $(6N + 10)$ order complex linear equation matrix is obtained, which can be used to determine the exact same number of unknown coefficients. N should be chosen large enough to lead to accurate results. In all the theoretical computations as given, $N = 40$ are used, unless otherwise specified. It should be noted that Equations (A.13), (A.16), and (A.17) with $J_{\tau,n}^{(3)}$ for $n = 0, 1, 2, \dots$ replaced by 0, together with Equations (A.7)–(A.10), are the equations which can be used to solve the wave diffraction problem of a piezoelectric WEC submerged in front of a bottom-seated breakwater [35].